

MRI image enhancement of the brain using U-NET

¹Pangestu Sandya Etniko Siagian, ²Eva Yulia Puspaningrum, ³Wan Suryani Wan Awang,

⁴I Gede Susrama Mas Diyasa*

^{1,2,4} Informatika, Ilmu Komputer, Universitas Pembangunan Nasional “Veteran” Jawa Timur,
Rungkut Madya Surabaya, Indonesia

³ Faculty of Informatics and Computing, University Sultan Zainal Abidin Besut Campus, 22200
Besut, Terengganu, Malaysia

*e-mail: igsusrama.if@upnjatim.ac.id

Abstract

The quality of Magnetic Resonance Imaging (MRI) images is often compromised by various types of noise, such as salt, pepper, salt-and-pepper, and speckle noise, caused by technical or environmental disturbances. This study aims to develop a brain MRI image denoising model based on the U-Net architecture, capable of effectively removing different types of noise. The methodology includes collecting normal brain MRI datasets, applying data augmentation to increase variability, and introducing artificial noise to simulate possible noise conditions. The U-Net model is trained and evaluated using the Mean Squared Error (MSE) and Peak Signal-to-Noise Ratio (PSNR) metrics. The novelty of this study lies in its combination of augmentation techniques, multi-intensity artificial noise variations, and its exclusive focus on normal brain MRI images. The results demonstrate that the U-Net model achieves optimal performance on salt-and-pepper noise at an intensity of 0.1, marked by the highest PSNR value of 37.2047 dB and the lowest MSE value of 0.000207. Conversely, the model shows the lowest performance on high-intensity speckle noise, indicating greater challenges in addressing multiplicative noise. This study contributes a systematic and empirically tested approach to improving the quality of brain MRI images with high efficiency, supporting the development of image-based diagnostic systems in the medical field.

Keywords: Deep Learning, Denoising, Image Enhancement, Noise, U-Net.

1 INTRODUCTION

In the medical field, medical imaging plays a vital role in assisting healthcare professionals in disease diagnosis and health condition analysis. Medical images represent two-dimensional patterns that visualize the internal structure of the human body. Among the various available medical imaging techniques, one of the most frequently utilized methods is Magnetic Resonance Imaging (MRI), which uses magnetic fields to produce detailed images of organs and body tissues [1].

However, the quality of MRI images is often compromised by the presence of noise or artifacts. These artifacts can hinder accurate diagnostic interpretation by medical professionals, creating the need for effective image enhancement methods. Image quality degradation can occur during the MRI acquisition process, where unwanted elements such as noise or artifacts may appear [2]. Digital image enhancement techniques are thus crucial for improving image clarity and usability, enabling healthcare professionals to better understand human anatomy and make accurate diagnoses. Poor-quality medical images can lead to inaccurate assessments of a patient's health condition, potentially affecting treatment decisions.

Various approaches have been employed for noise reduction (denoising), including traditional methods such as spatial domain filtering, variational denoising, and transform domain filtering. Modern approaches, such as machine learning, refer to the ability of systems to learn from specific training data to produce analytical models capable of performing designated tasks. The addition of noise is used to enhance the model's feature extraction capability. By training the model on data with added noise, the model can learn to extract key features from noisy images, thus improving its overall performance [3].

2 LITERATURE REVIEW

A study conducted in 2024 [4] employed a contrast enhancement algorithm to improve the quality of X-ray images, thereby assisting medical professionals in making more accurate diagnoses and treatment decisions. The research proposed a contrast enhancement approach that considers the local characteristics of X-ray images. The method involves dividing the image into small fragments, then applying different contrast enhancement algorithms to each fragment. Each fragment is evaluated based on the Root Mean Square (RMS) criterion, and the algorithm that yields the highest RMS value is selected as the optimal algorithm for that fragment.

Another study in 2024 examined various denoising algorithms used to remove noise in MRI images [5]. MRI is often affected by random noise that can be modeled as Gaussian or Rician distributions. This study reviewed multiple existing denoising algorithms and found that the Non-Local Means (NLM) filter performed better than other established methods. Additionally, it explored improvements to the NLM approach. The evaluation showed that combining Principal Component Analysis (PCA) with NLM resulted in superior performance both quantitatively and qualitatively.

A 2023 study [6] implemented a denoising method specifically for brain MRI images. To address the problem of noise in medical images, the study utilized a Convolutional Denoising Autoencoder (CDAE) as the method for removing noise from brain MRI images. CDAE was chosen for its ability to extract important information while preserving spatial details of the image, resulting in more accurate and efficient denoising. The model evaluation demonstrated strong performance, with a Structural Similarity Index Measure (SSIM) of 0.85 and a Peak Signal-to-Noise Ratio (PSNR) of 30 dB.

In 2021, a study [7] aimed to eliminate noise caused by technical or environmental errors. Denoising not only improves image quality but also facilitates other image processing tasks. However, classical denoising techniques were considered less efficient and flexible. Therefore, the study compared two promising neural network architectures for tackling these issues: Autoencoder and U-Net. The study implemented and evaluated several models of both architectures using a preprocessed dataset. The evaluation used standard image quality metrics, namely PSNR and SSIM. Experimental results showed that the U-Net model produced better denoised images compared to the basic Autoencoder. The outputs of the Autoencoder were generally blurry, whereas the skip-connections in U-Net effectively preserved image details, resulting in higher PSNR and SSIM values.

The main research gap identified from previous studies is the lack of investigations that explicitly induce various types of artificial noise such as salt noise, pepper noise, salt-and-pepper noise, and speckle noise into MRI datasets and then use the U-Net architecture to handle each noise type. Moreover, model performance in removing various types of noise has not been systematically evaluated using quantitative metrics such as Mean Squared Error (MSE) and Peak Signal-to-Noise Ratio (PSNR) [8]. Therefore, this study aims to develop a model capable of enhancing medical images degraded due to technical or environmental disturbances.

3 RESEARCH METHODOLOGY

This research is structured to ensure a systematic process from start to finish. The methodology serves as a guide for organizing each stage of the study, from data collection, augmentation, artificial noise induction, development of the U-Net deep learning-based model, to the evaluation phase. This workflow is designed so that every phase aligns with the research objective—particularly in developing an effective and accurate brain MRI image denoising system. [Figure 1](#) further supports this explanation by visually illustrating the stages of the research process.

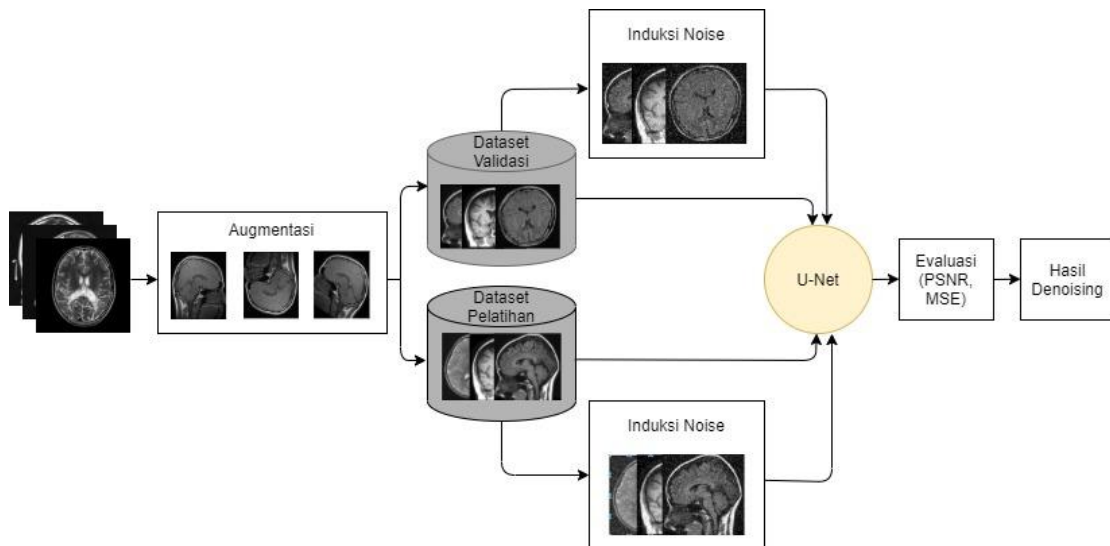


Figure 1. Research Methodology

3.1 Data collection

This step in the research involves collecting brain MRI images from a Kaggle dataset called “Crystal Clean: Brain Tumors MRI Dataset.” This dataset consists of two main categories: normal brain MRI images and brain MRI images with tumors. For this study, only normal brain MRI images will be utilized. The use of normal images as the focus of this research allows for a more controlled evaluation of the effectiveness of the U-Net model. The dataset includes three types of human head orientations based on the fundamental MRI imaging planes: side view (sagittal plane), front-to-back view (coronal plane), and top-to-bottom view (axial plane) [9] [10], as shown in [Figure 2](#), which sequentially displays examples from this MRI dataset.

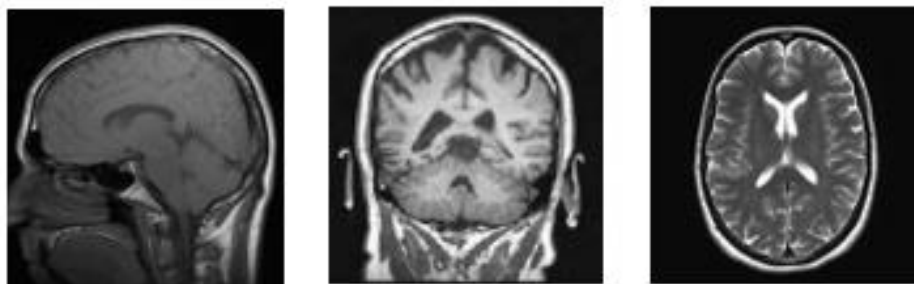


Figure 2. Sample of Brain MRI Dataset

[Figure 2](#) is, the MRI images used in this study are in “jpg” format. For the purpose of model training, a total of 417 normal brain MRI images were collected as training data. This substantial sample size enables the model to learn various patterns and structural features present in normal brain MRI images. Additionally, to comprehensively evaluate the model's performance, 104 normal brain MRI images were used as validation data. The use of a separate validation dataset ensures an objective assessment of the model's generalization ability on unseen images.

3.2 Augmentation

Augmentation is a crucial step in this research to increase the variability of the training data without the need for additional data collection [11][12]. This process includes quality control of the data to ensure the integrity of the dataset, standardization of image resolution to a uniform size of 255x255 pixels, and conversion of the images to grayscale format. The process involves modifying the brain MRI images using various augmentation techniques, such as brightness adjustment, darkening, horizontal/vertical flipping, and rotation. The goal of this process is to improve the model's generalization, reduce the risk of overfitting, and allow the model to recognize important features more accurately despite variations in visual disturbances such as noise [13]. This approach strengthens the model's resilience to handle complex and diverse data, enabling it to deal with various variations in input data. Augmentation aims to enhance the model's generalization by simulating real-world conditions with varied characteristics [14][15].

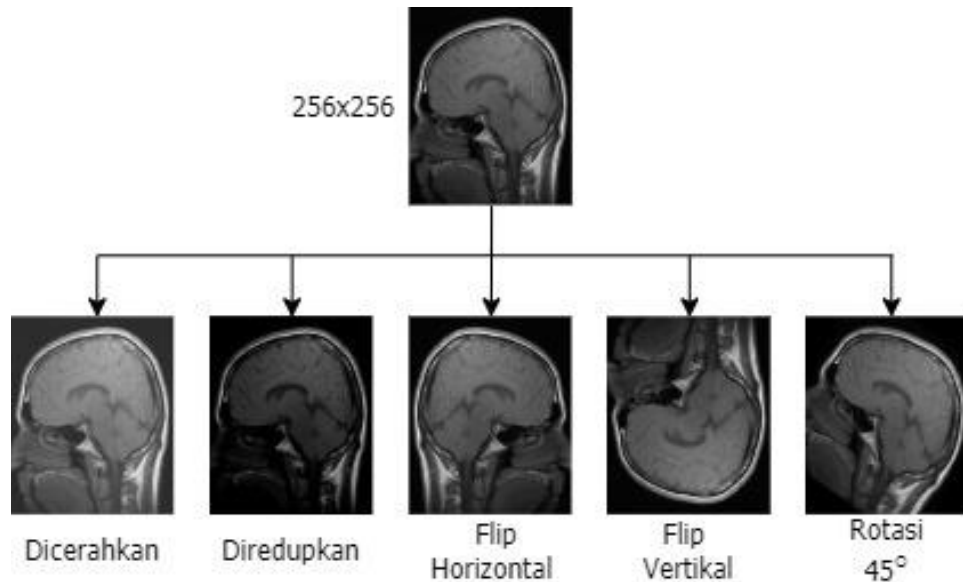


Figure 3. Sample of Brain MRI Dataset

[Figure 3](#) is After augmentation using five methods, the training dataset increased to 2,085 samples, and the validation dataset increased to 520 samples. The data split ratio for this process was 80:20 from the 2,605 MRI images. This split is a common practice in machine learning model development, providing a good balance between sufficient training data and a representative sample for validation [\[16\]\[17\]](#). By using a validation set during training, researchers can monitor metrics such as MSE and PSNR to detect issues such as overfitting or underfitting, and make necessary model parameter adjustments.

3.3 Noise Induction

Artificial noise was added to the brain MRI images as part of the training and validation phases of the model [\[18\]](#). The main purpose of adding this noise is to simulate real-world conditions where MRI images may be disturbed by various factors, such as magnetic field interference, patient movement, or hardware limitations. Since MRI images with artifacts are difficult to obtain, adding artificial noise becomes an important strategy to create representative training data. In this way, the model can learn to recognize and remove noise, improving its ability to restore image quality and maintain the diagnostic value of medical images.

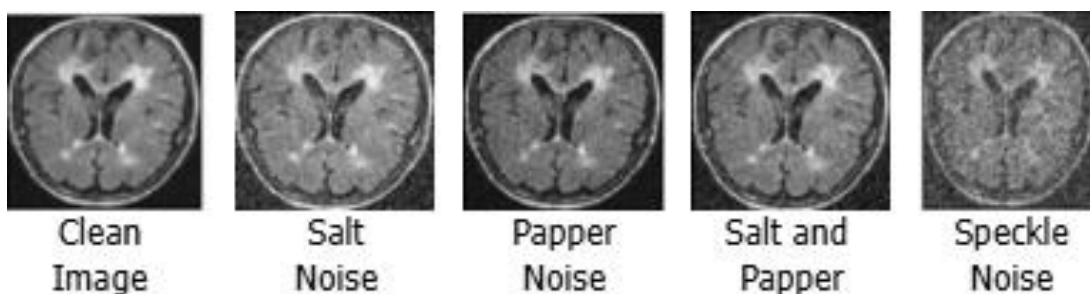


Figure 4. Noise Induction

The addition of artificial noise types such as Salt Noise, Pepper Noise, Salt & Pepper Noise, and Speckle Noise aims to create realistic challenges for the model during the denoising process, as shown in [Figure 4](#). The result of this stage is two datasets: the training data and the validation data, each consisting of both clean and noisy versions, as illustrated in [Figure 5](#). This approach allows the model to learn comprehensively from various image conditions, thereby improving the model's generalization ability and effectiveness in removing noise from brain MRI images [\[19\]](#).

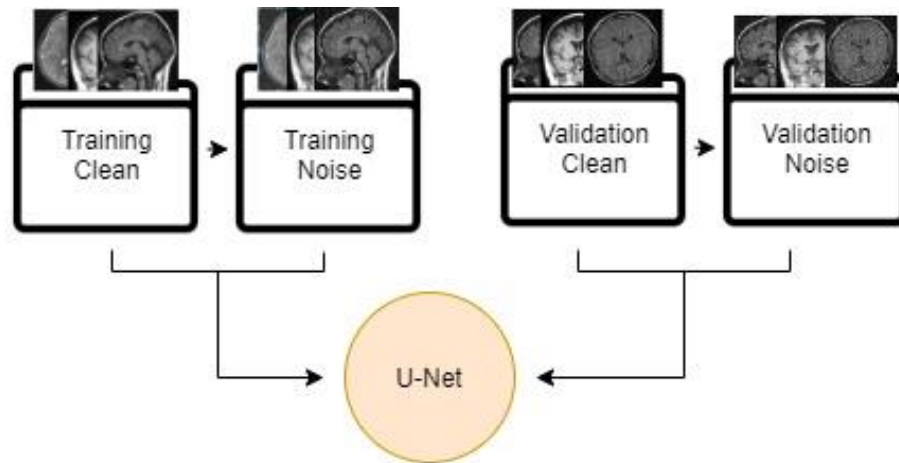


Figure 5. Clean and Noisy Data Sets

3.4 U-Net Architecture

The U-Net architecture designed in this study is specifically used for the task of image denoising, which is the process of removing noise from input images to recover clean and high-quality images [20]. U-Net is a type of convolutional neural network (CNN) architecture that has proven effective in various image processing applications, especially in the medical field. One of the main advantages of U-Net lies in its symmetric structure, which consists of an encoder and decoder path, allowing the model to capture both local and global features effectively.

Additionally, U-Net is equipped with skip-connections—direct links between layers in the contracting path and layers in the expanding path. This mechanism is crucial as it helps retain spatial information, which is often lost during the downsampling process. In the context of denoising [20], the ability to preserve spatial details is critical to ensure that the final image remains sharp and does not lose important structures, especially in medical images such as brain MRI scans. The illustration of the U-Net architecture used can be seen in [Figure 6](#).

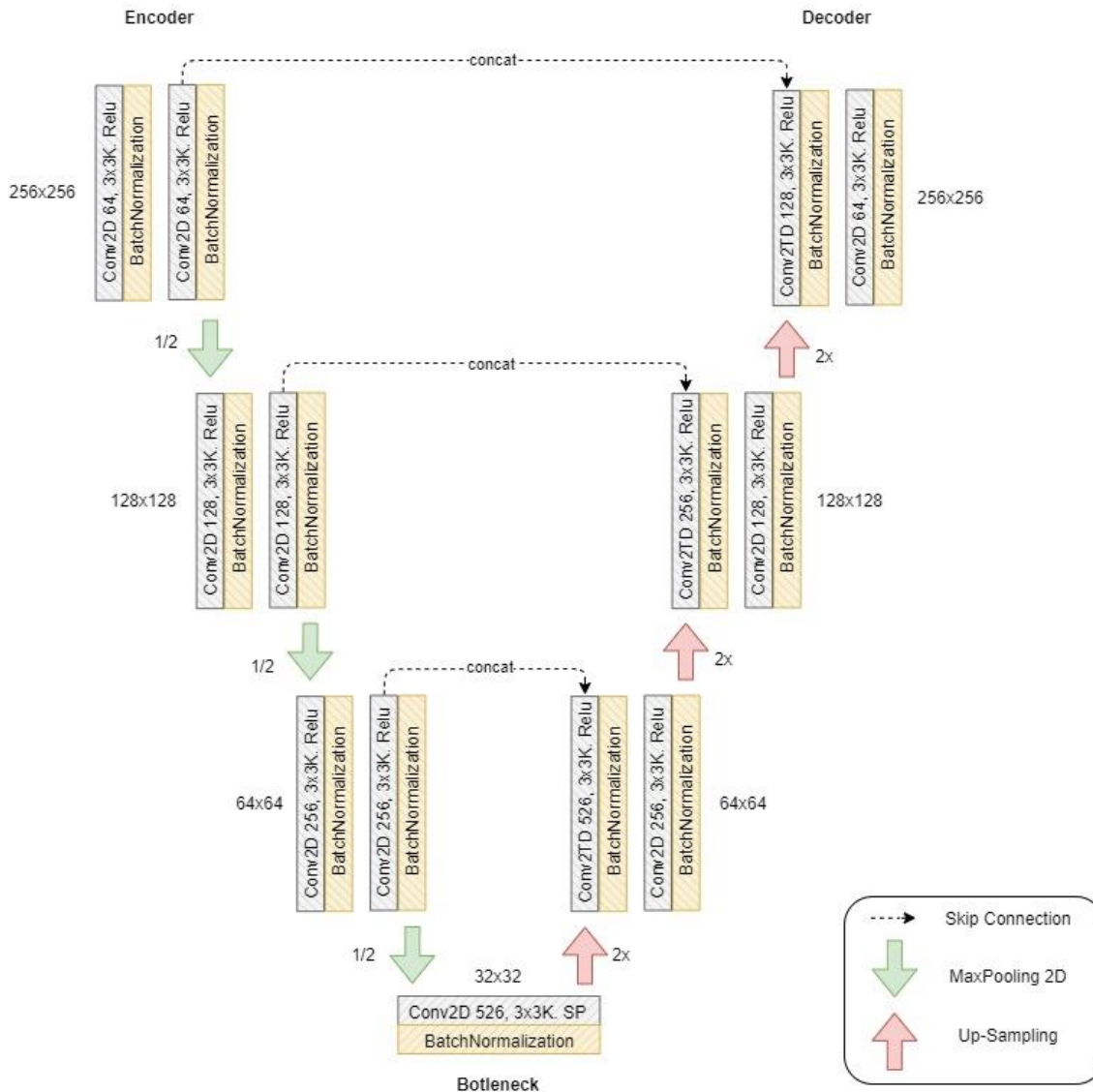


Figure 6. U-Net Architecture

In [Figure 6](#), the U-Net architecture consists of three main parts: the encoder (contracting path), the bottleneck, and the decoder (expansive path). The encoder is responsible for extracting important features from the input image [\[21\]](#), where the input image has a size of 256×256 pixels with one channel (grayscale). This process is done step-by-step through convolutional blocks and downsampling. Each block consists of two Conv2D layers with the number of filters sequentially set to 64, 128, and 256, a kernel size of 3×3, padding “same,” and ReLU activation, each followed by Batch Normalization to stabilize activation distribution and speed up the training process. After two convolutional layers, a MaxPooling2D process with a 2×2 size is applied to reduce spatial dimensions while retaining important features of the image.

The bottleneck layer is located at the innermost part of the network and serves as the most compact and meaningful feature representation [\[22\]](#). In this section, two Conv2D layers with 526 filters, a 3×3 kernel, “same” padding, and ReLU activation are used, each followed by Batch Normalization. There is no downsampling or upsampling in this section.

After the bottleneck, the decoder part reconstructs the image from the compact feature representation back into its original spatial form [\[23\]](#). This process is done through upsampling with a 2×2 factor by Conv2DTranspose to increase spatial dimensions. Each decoder block consists of one Conv2DTranspose layer and one Conv2D layer, with filters sequentially set to 256, 128, and 64. Each layer uses a 3×3 kernel, “same” padding, and ReLU activation, followed by Batch Normalization. To retain important spatial information from the encoder, skip-connections are used to concatenate features from the corresponding encoder layer to the decoder

layer at the same resolution. Finally, the output layer uses Conv2D with a 1×1 kernel and sigmoid activation to generate the output image with pixel values in the range $[0,1]$. This model is compiled using the Adam optimizer and MSE loss function for image reconstruction and denoising tasks.

3.5 Testing Scenario

This study uses an evaluative approach to assess the effectiveness of the U-Net model in removing various types of noise from brain MRI images. In the testing phase, four types of artificial noise are used: Salt, Pepper, Salt & Pepper, and Speckle Noise, each tested at three levels of variance (0.05, 0.10, and 0.15) [24]. These variances represent the level of disturbance in the images, either in the form of the proportion of pixels affected by noise (for Salt, Pepper, and Salt & Pepper) or the intensity of multiplicative noise (for Speckle Noise), as shown in [Table 1](#).

Table 1. Testing Parameters

Parameter	Value
Noise	<i>Salt, Pepper, Salt and Pepper, Speckle</i>
Variance	0,05; 0,1; 0,15
Evaluation Metric	MSE, PSNR

The model is trained using the Mean Squared Error (MSE) loss function, which aims to minimize the difference between the reconstructed image and the original image. In addition, the PSNR metric is also used to evaluate the quality of the reconstruction results. A high PSNR indicates a low level of disturbance and better image quality [25]. With a training configuration that includes a small batch size, such as 8, a relatively low number of epochs, such as 20, and the use of the ADAM optimizer, this study aims to balance training efficiency and model accuracy. This strategy allows for a quick assessment of the model's performance, as well as helps identify the strengths and weaknesses of U-Net in handling specific types of noise.

$$MSE = \frac{1}{w \times h} \sum_{i=0}^{w-1} \sum_{j=0}^{h-1} (I(i,j) - K(i,j))^2 \quad (1)$$

The Mean Squared Error (MSE) in [equation \(1\)](#) is one of the most commonly used evaluation metrics to assess image reconstruction quality in various digital image processing applications. This metric calculates the average of the squared differences between the pixel intensities of the original image and the reconstructed image. A lower MSE value indicates that the reconstruction result has a small error compared to the original image, thus it is considered to have better quality [26]. On the other hand, a high MSE value indicates a significant difference between the original image and the reconstructed result, which reflects a degradation in quality.

$$PSNR = 10 \times \log_{10} \frac{(data\ range)^2}{MSE} \quad (2)$$

The Peak Signal-to-Noise Ratio (PSNR) in [equation \(2\)](#) is a metric used to measure image reconstruction quality by comparing the original image with the reconstructed image. PSNR represents the ratio between the maximum signal strength of the original image and the strength of noise that degrades the image representation. A higher PSNR value indicates that the reconstructed image has lower distortion, thus the image quality is better and closer to the original image [26]. A high PSNR value indicates that the reconstructed image has visual quality similar to the original image, with minimal distortion. PSNR values above 30 dB are generally considered good, as high image quality is crucial for accurate medical diagnosis purposes [27]. On the other hand, PSNR values below 20 dB often reflect significant distortion, where the image becomes blurry or heavily affected by noise, potentially interfering with visual interpretation [27][28].

4 RESULTS AND DISCUSSION

Table 2. Training and Validation Loss Curve Graph

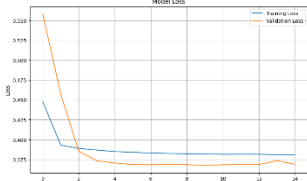
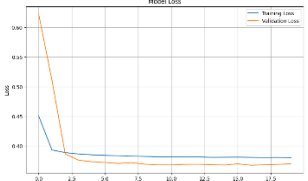
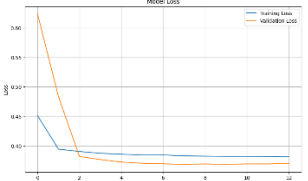
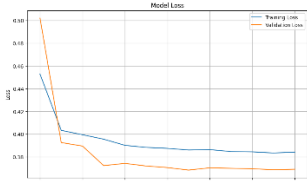

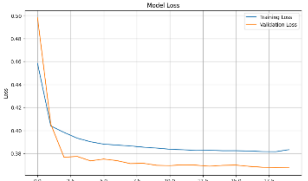
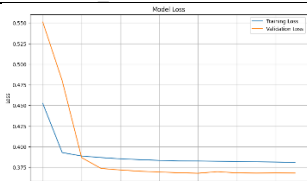
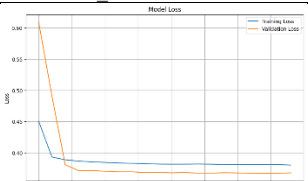
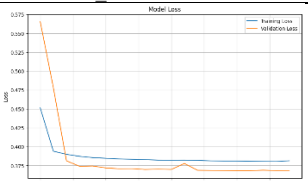
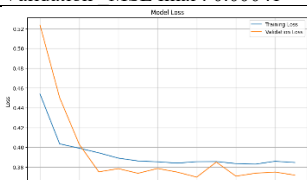
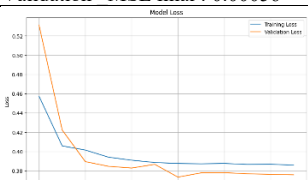
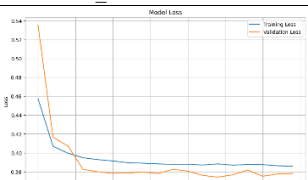
Noise Type	Intensity		
	0,05	0,1	0,15
<i>Salt</i>	 <p>Training_MSE first: 0.0453 Training_MSE final : 0.00074 Validation_MSE first: 0.0633 Validation_MSE final: 0.00029</p>	 <p>Training_MSE first: 0.0462 Training_MSE final : 0.00043 Validation_MSE first: 0.0935 Validation_MSE final : 0.00032</p>	 <p>Training_MSE first: 0.0473 Training_MSE final : 0.00071 Validation_MSE first: 0.0943 Validation_MSE final : 0.00063</p>
<i>Pepper</i>	 <p>Training_MSE first : 0.0415 Training_MSE final : 0.0015 Validation_MSE first : 0.0388 Validation_MSE final : 0.00035</p>	 <p>Training_MSE first : 0.0437 Training_MSE final : 0.00088 Validation_MSE first : 0.0392 Validation_MSE final : 0.00022</p>	 <p>Training_MSE first : 0.0455 Training_MSE final : 0.00083 Validation_MSE first : 0.0370 Validation_MSE final : 0.0003</p>
<i>Salt and Pepper</i>	 <p>Training_MSE first : 0.0451 Training_MSE final : 0.00054 Validation_MSE first : 0.0595 Validation_MSE final : 0.00041</p>	 <p>Training_MSE first : 0.0463 Training_MSE final : 0.00048393 Validation_MSE first : 0.0869 Validation_MSE final : 0.00056</p>	 <p>Training_MSE first : 0.0490 Training_MSE final : 0.00079 Validation_MSE first : 0.0660 Validation_MSE final : 0.00038</p>
<i>Speckle</i>	 <p>Training_MSE first : 0.0462 Training_MSE final : 0.0014 Validation_MSE first : 0.0479 Validation_MSE final : 0.00068</p>	 <p>Training_MSE first : 0.0458 Training_MSE final : 0.0015 Validation_MSE first : 0.0504 Validation_MSE final : 0.0014</p>	 <p>Training_MSE first : 0.0481 Training_MSE final : 0.0016 Validation_MSE first : 0.0524 Validation_MSE final : 0.0018</p>

Table 2 presents the training loss curve (blue line) and validation loss curve (yellow line) of the U-Net model for each type of noise—namely Salt, Pepper, Salt and Pepper, and Speckle—at three different intensity levels (0.05, 0.1, and 0.15). The Y-axis in the graph represents the MSE value, while the X-axis represents the number of epochs. Overall, the declining pattern of MSE loss indicates that the model successfully performed the learning process, as evidenced by the consistent decrease in both training and validation loss as the number of epochs increases.

As shown in [Table 2](#), for Salt noise, the model exhibits a sharp loss reduction at the beginning of training and stabilization in the subsequent epochs, both for training and validation data. This significant reduction reflects the model's ability to extract relevant features early in the learning process, even though the images have been contaminated by impulsive unipolar noise such as Salt.

The loss curve pattern for Pepper noise, although showing slight fluctuations in the validation loss curve—particularly at intensities of 0.1 and 0.15 as seen in [Table 2](#)—may indicate variations in the model's generalization capability against this type of noise. These fluctuations suggest a

variation in the model's ability to generalize to Pepper noise, which is characterized by random dark spots in the image.

In the case of Salt and Pepper noise, [Table 2](#) shows that the loss curves exhibit a similar pattern to those of the Salt noise. This indicates good performance, as reflected in the rapid and consistent decrease in both training and validation loss throughout the training process. The parallel decline in loss values between the training and validation data indicates that the model not only adapts well to the training data but also maintains its generalization ability on unseen data.

Meanwhile, for Speckle noise, the curves show slightly more significant fluctuations in validation loss, as seen in [Table 2](#), particularly at the lower intensity (0.05), which may suggest that this type of noise is more challenging to reconstruct consistently by the model, especially in terms of generalization. Overall, these graphs demonstrate that the U-Net model has stable learning capabilities to handle various types of noise, although differences in stability and convergence speed exist depending on the type and intensity of the noise used.

Table 3. Denoising Performance

Noise Type	PSNR			MSE		
	0,05	0,1	0,15	0,05	0,1	0,15
Salt	35,4287dB	37,4250dB	35,4003dB	0,000321	0,000193	0,000321
Papper	34,6990dB	36,7617dB	35.5391dB	0,000366	0,000223	0,000297
Salt and Papper	35,2931dB	37.2047dB	35.2127dB	0,000318	0,000207	0,000328
Speckle	32.4261dB	29.1379dB	27.5417dB	0,000593	0,001266	0,001831

[Table 3](#) presents the PSNR and MSE metrics for the four types of noise at three intensity levels: 0.05, 0.1, and 0.15. For Salt noise, the highest PSNR is achieved at the medium intensity level (0.1), reaching 37.43 dB, while the lowest MSE is also recorded at the same intensity, with a value of 0.000193. This indicates that the U-Net model is most effective at removing salt noise at moderate intensity, resulting in image reconstructions that are very close to the original. At the lower intensity level (0.05) with 35.43 dB and at the higher intensity (0.15) with 35.40 dB, the PSNR slightly decreases, accompanied by a minimal increase in MSE. This suggests that increasing noise intensity beyond the optimal threshold has only a minor impact on the final image quality.

In the Pepper noise row of [Table 3](#), it is observed that the PSNR peaks at intensity 0.15 with 35.54 dB, while the lowest MSE is obtained at intensity 0.1 with a value of 0.000223. Although the PSNR at low intensity (0.05) is slightly lower (34.70 dB), the overall PSNR range is relatively small, indicating that the model performs well in handling random black spots in the image.

For the Salt and Pepper combination, the model's performance is nearly on par with that of the individual noise types. The highest PSNR is obtained at intensity 0.1 with 37.21 dB, and the lowest MSE is also at this level, with a value of 0.000207. The changes in PSNR and MSE across the three intensities are relatively consistent, suggesting that the model can reconstruct images effectively even when both noise types are present simultaneously. Similar to the loss curves, the performance results for Salt and Pepper noise closely resemble those of Salt noise alone.

In contrast, Speckle noise demonstrates the lowest performance among all noise types. The PSNR drops significantly as intensity increases—starting from 32.43 dB at 0.05 down to 27.54 dB at 0.15. The MSE rises sharply from 0.000593 to 0.001831. This indicates that Speckle noise, which is multiplicative and continuously distributed, poses a greater challenge for removal using the U-Net architecture, particularly at higher contamination levels.

5 CONCLUSION

Based on the analysis of the training and validation loss curves, as well as the evaluation metrics PSNR and MSE presented in [Tables 2](#) and [3](#), it can be concluded that the U-Net model has a strong capability in performing denoising on images contaminated by various types of noise. The model demonstrates the most optimal performance on impulsive noise types such as Salt, Pepper, and the combination of Salt and Pepper, particularly at moderate intensity levels (0.1), as indicated by high PSNR values and low MSE. Based on the analysis presented, Salt and Pepper noise at intensity 0.1 is the type of noise that is best handled by the U-Net model. This is reflected in the highest PSNR value of 37.2047 dB and the lowest MSE value of 0.000207, as shown in [Table 3](#). With a PSNR distortion above 30 dB, the noise can be effectively removed, and image details are preserved.

The results reflect the model's ability to extract important features and effectively reconstruct images, even with spatial disturbances. On the other hand, the model's performance significantly declines with Speckle noise, particularly at high intensity levels, which indicates that multiplicative and continuously distributed noise is more challenging to reduce by the U-Net architecture. In general, these results indicate that the efficiency of the U-Net model in the denoising process is highly influenced by the characteristics and intensity levels of the noise used, and it suggests that architectural adaptations or additional training strategies may be necessary to improve performance on more complex noise types.

This research opens up several promising directions for future studies. One potential development is enhancing the model architecture by adding extra regularization layers to improve the model's generalization and stability. Furthermore, the scope of the research could be expanded to include other types of noise commonly encountered in medical imaging, such as Poisson Noise (also known as Shot Noise) and Periodic Noise, which were not covered in this study. Heavier hyperparameter optimization strategies could also be explored, especially if more powerful computational resources are available. Although clinical implementation was not the main focus of this study, future research could examine the application of these denoising techniques in a clinical context, including real-time processing capabilities and integration with existing medical imaging workflows.

REFERENCES

- [1] B. Nouri, M. Arab, and M. Nasiri, "Endometriosis: Clinical, Magnetic Resonance Imaging and Pathologic Findings," *J. Obstet. Gynecol. Cancer Res.*, vol. 8, no. 5, pp. 481–487, Sep. 2023, doi: 10.30699/jogcr.8.5.481. <https://doi.org/10.30699/jogcr.8.5.481>
- [2] D. Tamada, "Review: *Noise* and artifact reduction for MRI using deep learning," Feb. 2020, [Online]. Available: <http://arxiv.org/abs/2002.12889> <https://doi.org/10.48550/arXiv.2002.12889>
- [3] A. Makhlof, M. Maayah, N. Abughanam, and C. Catal, "The use of generative adversarial networks in medical image augmentation," *Neural Comput. Appl.*, vol. 35, no. 34, pp. 24055–24068, Dec. 2023, doi: 10.1007/s00521-023-09100-z. <https://doi.org/10.1007/s00521-023-09100-z>
- [4] N. Mamatov, K. Erejepov, M. Jalelova, I. Narzullayev, and A. Samijonov, "X-ray Image Contrast Enhancement Approach," in 2024 3rd International Conference on Applied Artificial Intelligence and Computing (ICAAIC), IEEE, Jun. 2024, pp. 1293–1297. doi: 10.1109/ICAAIC60222.2024.10575386. <https://doi.org/10.1109/ICAAIC60222.2024.10575386>
- [5] A. Z. - and H. N. -, "A Study on Image *Noise* Removal Techniques for Magnetic Resonance Imaging," *Int. J. Multidiscip. Res.*, vol. 6, no. 1, Feb. 2024, doi: 10.36948/ijfmr.2024.v06i01.13298. <https://doi.org/10.36948/ijfmr.2024.v06i01.13298>
- [6] A. Thomas, D. K. K R, D. Babu, and A. P.E, "*Denoising Autoencoder* for the Removal of *Noise* in Brain MR Images," in 2023 International Conference on Control, Communication and Computing (ICCC), IEEE, May 2023, pp. 1–5. doi: 10.1109/ICCC57789.2023.10165274. <https://doi.org/10.1109/ICCC57789.2023.10165274>
- [7] M. Tripathi, "Facial image *denoising* using *Autoencoder* and UNET," *Herit. Sustain. Dev.*,

- vol. 3, no. 2, pp. 89–96, 2021, doi: 10.37868/hsd.v3i2.71.
<https://doi.org/10.37868/hsd.v3i2.71>
- [8] S.-H. Kang and Y. Lee, “Motion Artifact Reduction Using *U-Net* Model with Three-Dimensional Simulation-Based Datasets for Brain Magnetic Resonance Images,” *Bioengineering*, vol. 11, no. 3, p. 227, Feb. 2024, doi: 10.3390/bioengineering11030227.
<https://doi.org/10.3390/bioengineering11030227>
- [9] Y. Gi et al., “Study of multistep Dense *U-Net*-based automatic segmentation for head MRI scans,” *Med. Phys.*, vol. 51, no. 3, pp. 2230–2238, Mar. 2024, doi: 10.1002/mp.16824.
<https://doi.org/10.1002/mp.16824>
- [10] R. Touati, W. Trung Le, and S. Kadoury, “Multi-planar dual adversarial network based on dynamic 3D features for MRI-CT head and neck image synthesis,” *Phys. Med. Biol.*, vol. 69, no. 15, p. 155012, Aug. 2024, doi: 10.1088/1361-6560/ad611a.
<https://doi.org/10.1088/1361-6560/ad611a>
- [11] K.-J. Tsai, C.-C. Chang, L.-C. Lo, J. Y. Chiang, C.-S. Chang, and Y.-J. Huang, “Automatic segmentation of paravertebral muscles in abdominal CT scan by *U-Net*,” *Medicine (Baltimore)*, vol. 100, no. 44, p. e27649, Nov. 2021, doi: 10.1097/MD.00000000000027649.
<https://doi.org/10.1097/MD.00000000000027649>
- [12] M. Nishio, S. Noguchi, and K. Fujimoto, “Automatic Pancreas Segmentation Using Coarse-Scaled 2D Model of Deep Learning: Usefulness of Data Augmentation and Deep *U-Net*,” *Appl. Sci.*, vol. 10, no. 10, p. 3360, May 2020, doi: 10.3390/app10103360.
<https://doi.org/10.3390/app10103360>
- [13] O. Rainio and R. Klén, “Comparison of simple augmentation transformations for a convolutional neural network classifying medical images,” *Signal, Image Video Process.*, vol. 18, no. 4, pp. 3353–3360, 2024, doi: 10.1007/s11760-024-02998-5.
<https://doi.org/10.1007/s11760-024-02998-5>
- [14] D. Azcona, K. McGuinness, and A. F. Smeaton, “A Comparative Study of Existing and New Deep Learning Methods for Detecting Knee Injuries using the MRNet Dataset,” in *2020 International Conference on Intelligent Data Science Technologies and Applications (IDSTA)*, IEEE, Oct. 2020, pp. 149–155. doi: 10.1109/IDSTA50958.2020.9264030.
<https://doi.org/10.1109/IDSTA50958.2020.9264030>
- [15] W. Wu, M. Chen, Y. Xiang, Y. Zhang, and Y. Yang, “Recent progress in image *denoising*: A training strategy perspective,” *IET Image Process.*, vol. 17, no. 6, pp. 1627–1657, May 2023, doi: 10.1049/ipr2.12748.
<https://doi.org/10.1049/ipr2.12748>
- [16] S. S. Hidayat, D. Rahmawati, M. C. A. Prabowo, L. Triyono, and F. T. Putri, “Determining the Rice Seeds Quality Using Convolutional Neural Network,” *JOIV Int. J. Informatics Vis.*, vol. 7, no. 2, p. 527, Jun. 2023, doi: 10.30630/joiv.7.2.1175.
<https://doi.org/10.30630/joiv.7.2.1175>
- [17] T. Ashwin B. and B. Amma N. G., “Comparative Analysis of *Machine learning* Techniques for Classifying the Risk of Cardiovascular Diseases,” 2024, pp. 161–186. doi: 10.4018/979-8-3693-0683-3.ch009.
<https://doi.org/10.4018/979-8-3693-0683-3.ch009>
- [18] K. Ali, A. N. Qureshi, M. Shahid Bhatti, A. Sohail, M. Hijji, and A. Saeed, “De-Noising Brain MRI Images by Mixing Concatenation and Residual Learning (MCR),” *Comput. Syst. Sci. Eng.*, vol. 45, no. 2, pp. 1167–1186, 2023, doi: 10.32604/csse.2023.032508.
<https://doi.org/10.32604/csse.2023.032508>
- [19] X. Wang, Y. Hua, E. Kodirov, D. A. Clifton, and N. M. Robertson, “IMAE for *Noise*-Robust Learning: Mean Absolute Error Does Not Treat Examples Equally and Gradient Magnitude’s Variance Matters,” pp. 1–19, 2019, [Online]. Available: <http://arxiv.org/abs/1903.12141>
<https://doi.org/10.48550/arXiv.1903.12141>
- [20] J. Gurrola-Ramos, O. Dalmau, and T. E. Alarcon, “A Residual Dense *U-Net* Neural Network for Image *Denoising*,” *IEEE Access*, vol. 9, pp. 31742–31754, 2021, doi: 10.1109/ACCESS.2021.3061062.
<https://doi.org/10.1109/ACCESS.2021.3061062>
- [21] S. A. Naji and N. Majeed Saleh, “Digital Image Forgery Detection And Localization Using The Innovated *U-Net*,” *Iraqi J. Comput. Informatics*, vol. 50, no. 1, pp. 195–207, Jun. 2024, doi: 10.25195/ijci.v50i1.484.
<https://doi.org/10.25195/ijci.v50i1.484>

- [22] X. Li, H. Chen, D. Zheng, and X. Xu, “CED-Net: A more effective DenseNet model with channel enhancement,” *Math. Biosci. Eng.*, vol. 19, no. 12, pp. 12232–12246, 2022, doi: 10.3934/mbe.2022569. <https://doi.org/10.3934/mbe.2022569>
- [23] Y. Cui, X. Hong, H. Yang, Z. Ge, and J. Jiang, “AsymUNet: An Efficient Multi-Layer Perceptron Model Based on Asymmetric *U-Net* for Medical Image *Noise* Removal,” *Electronics*, vol. 13, no. 16, p. 3191, Aug. 2024, doi: 10.3390/electronics13163191. <https://doi.org/10.3390/electronics13163191>
- [24] W. El-Shafai et al., “Efficient deep-learning-based *Autoencoder denoising* approach for medical image diagnosis,” *Comput. Mater. Contin.*, vol. 70, no. 3, pp. 6107–6125, 2022, doi: 10.32604/cmc.2022.020698. <https://doi.org/10.32604/cmc.2022.020698>
- [25] L. Kong et al., “A Generalized Deep Learning Method for Synthetic CT Generation,” *Int. J. Radiat. Oncol.*, vol. 117, no. 2, p. e472, Oct. 2023, doi: 10.1016/j.ijrobp.2023.06.1681. <https://doi.org/10.1016/j.ijrobp.2023.06.1681>
- [26] Y. FAROOQ and S. SAVAŞ, “*Noise* Removal from the Image Using Convolutional Neural Networks-Based *Denoising Auto Encoder*,” *J. Emerg. Comput. Technol.*, vol. 3, no. 1, pp. 21–28, 2024, doi: 10.57020/ject.1390428. <https://doi.org/10.57020/ject.1390428>
- [27] Patrisius Batarius, Alfry Aristo Sinlae, and Elisabeth F. Fahik, “Analysis of the Quality of Natural Dyes in Weaving Exposed to Sunlight Using MSE and PSNR Parameters,” *J. RESTI (Rekayasa Sist. dan Teknol. Informasi)*, vol. 6, no. 5, pp. 797–802, Oct. 2022, doi: 10.29207/resti.v6i5.4339. <https://doi.org/10.29207/resti.v6i5.4339>
- [28] Y. Y. Al-Aboosi, R. S. Issa, and A. Khalid Jassim, “Image denosing in underwater acoustic *noise* using discrete wavelet transform with different *noise* level estimation,” *Telkomnika (Telecommunication Comput. Electron. Control.)*, vol. 18, no. 3, pp. 1439–1446, 2020, doi: 10.12928/TELKOMNIKA.V18I3.14381. <https://doi.org/10.12928/telkomnika.v18i3.14381>